

**Rapid hydrodynamic expansion in relativistic heavy-ion collisions**Piotr Bożek<sup>1,2,\*</sup> and Iwona Wyskiel<sup>1</sup><sup>1</sup>*The H. Niewodniczański Institute of Nuclear Physics, PL-31342 Kraków, Poland*<sup>2</sup>*Institute of Physics, Rzeszów University, PL-35959 Rzeszów, Poland*

(Received 24 February 2009; revised manuscript received 9 April 2009; published 30 April 2009)

Hydrodynamic expansion of the hot fireball created in relativistic Au-Au collisions at  $\sqrt{s} = 200$  GeV in  $3 + 1$ -dimensions is studied. We obtain a simultaneous, satisfactory description of the transverse momentum spectra, elliptic flow, and pion correlation radii for different collision centralities and different rapidities. Early initial time of the evolution is required to reproduce the interferometry data, which provide a strong indication of the early onset of collectivity. We can also constrain the shape of the initial energy density in the beam direction, with a relatively high initial energy density at the center of the fireball.

DOI: [10.1103/PhysRevC.79.044916](https://doi.org/10.1103/PhysRevC.79.044916)

PACS number(s): 25.75.Dw, 25.75.Ld

**I. INTRODUCTION**

A multitude of experimental data from the Relativistic Heavy Ion Collider (RHIC) indicate that dense, collectively expanding matter is created in ultrarelativistic nuclear collisions [1–4]. Ratios of multiplicities of different particles produced in central collisions can be described assuming chemical equilibration of particle abundances [5–10]. Transverse momentum spectra of particles produced at central rapidities are thermal up to transverse momenta of about 2 GeV/c. Particle spectra result from a collective, transverse expansion of the matter coupled with subsequent thermal emission [11,12]. Possible rescattering and resonance decays have been modelled and the conclusion, that at some stage of the expansion a dense locally equilibrated fireball is formed, remains unchanged [13,14]. Another measured quantity directly resulting from the collective expansion is the elliptic flow. For non-zero impact parameters the fireball is azimuthally asymmetric in the transverse plane, and its expansion imprints the momentum distribution of final hadrons with measurable azimuthal asymmetry [15–18]. The existence of the dense matter is demonstrated in yet another way by the observation of the attenuation of the production of high energy hadrons in nuclear collisions. This effect is due to the energy loss of energetic partons while traversing the dense fireball [19–24].

Relativistic hydrodynamics is very well suited for the description of the collective phase of the fireball expansion [14,16,25–37]. Assuming local thermal equilibration, perfect fluid hydrodynamics can be used. Starting from an initial energy density profile, the fluid expands and cools down. In the process, gradients of the pressure cause the acceleration of the fluid elements and collective flow velocity is formed. In the longitudinal (beam) direction Bjorken flow with velocity  $v_z = z/t$  is usually assumed in the initial conditions. On the other hand, the appearance of a substantial transverse flow can be considered as a robust signature of the formation of strongly interacting matter in the overlap region of heavy-ion collisions. Most of the hydrodynamic calculations modeling nuclear collisions at RHIC energies assume boost-invariance

[38] in the beam direction. Such approaches are effectively  $2 + 1$ -dimensional ( $2 + 1D$ ) and are restricted to central rapidities. Existing experimental data outside of the central rapidity region on particle multiplicity and elliptic flow show that at RHIC energies the Bjorken boost-invariance is not realized. Calculations exist for the general  $3 + 1D$  geometry of the collision [14,27,28,31,36]. They show that relativistic hydrodynamics can be applied for a broad range of rapidities in central and semiperipheral collisions. These studies can describe transverse momentum spectra and the elliptic flow of produced particles. On the other hand, Hanbury Brown–Twiss (HBT) correlations between identical particles cannot be accounted for [27,39–41]. In the present paper we investigate  $3 + 1D$  hydrodynamic expansion of the fireball and show that a simultaneous and satisfactory description of the particle spectra and elliptic flow (for a broad range of rapidities) as well as of the HBT radii for central rapidities can be achieved. The key ingredients of the model leading to this success are the use of a realistic equation of state without a first order phase transition and a relatively early start up time for the collective expansion. This hard equation of state and the small initial time indicate that the initial state is a highly compressed matter with energy density of up to 100 GeV/fm<sup>3</sup> in central collisions. In this work we use perfect fluid hydrodynamics. Shear viscosity or hadronic dissipative effects are known to modify final observables [33,34,42–47], especially the elliptic flow. The influence of viscosity effects on particle spectra or HBT radii is more difficult to be explicitly demonstrated, since such effects can be compensated by a change in the unknown initial time or energy density profile.

**II. HYDRODYNAMIC EQUATIONS AND INITIAL CONDITIONS**

In a perfect fluid each element is locally in thermal equilibrium. At each point the fluid is characterized by its four velocity  $u^\mu$ , the energy density  $\epsilon$ , and the pressure  $p$ . The energy momentum tensor is

$$T^{\mu\nu} = (\epsilon + p)u^\mu u^\nu - g^{\mu\nu} p. \quad (2.1)$$

\*Piotr.Bozek@ifj.edu.pl

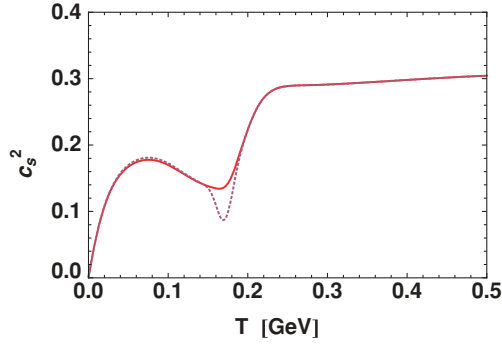


FIG. 1. (Color online) Temperature dependence of the velocity of sound squared [48]. The solid line corresponds to the default equation of state used, whereas the dashed line represents an equation with a soft point around  $T_c = 170$  MeV.

### Hydrodynamic equations

$$\partial_\mu T^{\mu\nu} = 0 \quad (2.2)$$

in the full 3+1D geometry represent four independent equations, and together with the equation of state allow to calculate the evolution of the densities and velocities of the fluid starting from some initial conditions. We use a realistic equation of state interpolating between lattice data at high temperature (above the critical temperature  $T_c = 170$  MeV) and an equation of state of a noninteracting gas of massive hadrons at lower temperatures [48]. This equation of state presents only a very moderate softening around the critical point (solid line in Fig. 1). The use of this realistic equation of state is the key to the success of 2 + 1D hydrodynamic description of RHIC data on transverse momentum spectra, elliptic flow and HBT radii [26,49]. In the Appendix, results obtained with an equation of state giving a reduction of the sound velocity around  $T_c$  (dashed line in Fig. 1) are shown for comparison. In the description of the dynamics of matter at very forward and backward rapidities the effects of significant, rapidity dependent baryon chemical potential may become important. Estimates from statistical model fits [50,51] show that at nonzero rapidities the baryon content in the fluid is growing. To describe it in a fluid dynamics framework an additional equation for the baryon current should appear, and an equation of state depending on the baryon density must be used. In the present work we use a lattice QCD inspired equation of state [48], for which only data a zero baryon density exists. Therefore we calculate a baryon-free hydrodynamic evolution, with the caution that at large rapidities the description becomes less reliable.

For the modeling of the expansion of the fireball created in ultrarelativistic collisions it is useful to define the proper time and space-time rapidity variables

$$\tau = \sqrt{t^2 - z^2}, \quad \eta = \frac{1}{2} \log \left( \frac{t+z}{t-z} \right), \quad (2.3)$$

with  $z$  the beam axis coordinate. The four velocity is parametrized using the two components of the transverse velocity  $u_x$  and  $u_y$  and the longitudinal fluid rapidity  $Y$

$$u^\mu = (\gamma \cosh Y, u_x, u_y, \gamma \sinh Y), \quad (2.4)$$

where  $\gamma = \sqrt{1 + u_x^2 + u_y^2}$ . Hydrodynamic equations relate four unknown functions: the velocity fields  $Y$ ,  $u_x$ , and  $u_y$  and either the energy or the pressure. In practice the numerical solution is more stable if instead of the energy density (pressure) the logarithm of the temperature is used

$$\mathcal{F} = \log(T/T_L), \quad (2.5)$$

with  $T_L$  a constant temperature. The velocities and  $\mathcal{F}$  are function of  $\tau$ ,  $\eta$ ,  $x$ ,  $y$  and the hydrodynamic equations can be written in the following form:

$$\begin{aligned} D\mathcal{F} &= -c_s^2 \left[ \gamma \left( \sinh(Y - \eta) \partial_\tau + \frac{\cosh(Y - \eta)}{\tau} \partial_\eta \right) Y \right. \\ &\quad \times \left( \cosh(Y - \eta) \partial_\tau + \frac{\sinh(Y - \eta)}{\tau} \partial_\eta \right) \gamma \\ &\quad \left. + \partial_x u_x + \partial_y u_y \right], \\ Du_x &= -(1 + u_x^2) \partial_x \mathcal{F} - u_x u_y \partial_y \mathcal{F} \\ &\quad - u_x \gamma \left( \cosh(Y - \eta) \partial_\tau + \frac{\sinh(Y - \eta)}{\tau} \partial_\eta \right) \mathcal{F}, \\ Du_y &= -(1 + u_y^2) \partial_y \mathcal{F} - u_x u_y \partial_x \mathcal{F} \\ &\quad - u_y \gamma \left( \cosh(Y - \eta) \partial_\tau \right. \\ &\quad \left. + \frac{\sinh(Y - \eta)}{\tau} \partial_\eta \right) \mathcal{F}, \\ D(\gamma \sinh Y) &= -\cosh Y \left[ \sinh(Y - \eta) \partial_\tau + \frac{\cosh(Y - \eta)}{\tau} \partial_\eta \right. \\ &\quad \left. + (u_x^2 + u_y^2) \left( \cosh(Y - \eta) \partial_\tau \right. \right. \\ &\quad \left. \left. + \frac{\sinh(Y - \eta)}{\tau} \partial_\eta \right) \right] \mathcal{F} \\ &\quad - \gamma \sinh Y (u_x \partial_x + u_y \partial_y) \mathcal{F}, \end{aligned} \quad (2.6)$$

where  $c_s$  is the sound velocity and

$$\begin{aligned} D &= u^\mu \partial_\mu = u_x \partial_x + u_y \partial_y \\ &\quad + \gamma \left( \cosh(Y - \eta) \partial_\tau + \frac{\sinh(Y - \eta)}{\tau} \partial_\eta \right). \end{aligned} \quad (2.7)$$

The first of Eqs. (2.6) is the entropy conservation equation  $\partial_\mu(u^\mu s) = 0$ .

The differential equations (2.6) are solved as an evolution in proper time starting from some initial conditions at  $\tau = \tau_0$ . At the initial time there is no transverse flow ( $u_x = 0$  and  $u_y = 0$ ), the initial longitudinal rapidity follows the Bjorken scaling flow  $Y(\tau_0, \eta, x, y) = \eta$ . Early initial time of the hydrodynamic evolution  $\tau_0 = 0.25$  fm/c implies a high energy density in the initial state. The system evolves for a longer time, which leads to a stronger transverse as well as longitudinal flow. Experimental observation of a strong rapidity dependence of the elliptic flow [52] and of the particle densities [53] indicates that the Bjorken scaling scenario is not realized at RHIC energies. It means that a Bjorken scaling plateau in the initial energy density distribution in space-time rapidity

cannot extend over a large interval. To illustrate this effect, we present in the Appendix A results obtained with initial conditions having a broader distribution in space-time rapidity, leading to an incorrect shape of the pseudorapidity dependence of the elliptic flow. In the transverse plane the energy density is assumed to be proportional to a combination of Glauber model densities of wounded nucleons and binary collisions. The initial energy density distribution at impact parameter  $b$  is

$$\epsilon(\tau_0) = kf(\eta - \eta_{sh}) [(N_A(x, y) + N_B(x, y))(1 - \alpha) + 2\alpha N_{\text{bin}}(x, y)]. \quad (2.8)$$

$N_A$  and  $N_B$  are the densities of wounded nucleons from the right and left moving nuclei, respectively,  $N_{\text{bin}}$  is the density of binary collisions

$$\begin{aligned} N_A(x, y) &= T(x - b/2, y)(1 - \exp(-\sigma T(x+b/2, y)/A)), \\ N_B(x, y) &= T(x + b/2, y)(1 - \exp(-\sigma T(x-b/2, y)/A)), \\ N_{\text{bin}}(x, y) &= \sigma T(x - b/2, y)T(x + b/2, y), \end{aligned} \quad (2.9)$$

and

$$T(x, y) = \int dz \rho(x, y, z) \quad (2.10)$$

is the thickness function calculated from the Woods-Saxon density of colliding nuclei

$$\rho(x, y, z) = \frac{\rho_0}{1 + \exp((\sqrt{x^2 + y^2 + z^2} - R_A)/a)}. \quad (2.11)$$

For Au nuclei ( $A = 197$ ) we take  $\rho_0 = 0.17 \text{ fm}^{-3}$ ,  $R_A = 6.38 \text{ fm}$ , and  $a = 0.535 \text{ fm}$ ; the inelastic cross section is  $\sigma = 42 \text{ mb}$ . The density of wounded nucleons  $N_A + N_B$  is used to calculate the total number of participants at each impact parameter, these numbers are used to fix the impact parameters corresponding to centrality bins used in the analysis of the experimental data. The profile in the longitudinal direction is

$$f(\eta) = \exp\left(-\frac{(\eta - \eta_0)^2}{2\sigma_\eta^2} \theta(|\eta| - \eta_0)\right) \quad (2.12)$$

with a plateau of width  $2\eta_0 = 2.0$  units in space-time rapidity, and Gaussian tails with half-width  $\sigma_\eta = 1.3$ . At each point in the transverse plane the distribution in space-time rapidity is shifted by the center of mass rapidity of the local fluid [27]

$$\eta_{sh} = \frac{1}{2} \log\left(\frac{N_A + N_B + v_N(N_A - N_B)}{N_A + N_B - v_N(N_A - N_B)}\right), \quad (2.13)$$

where  $v_N$  is the velocity of the projectile in the center of mass frame. The coefficient of  $k$  in Eq. (2.8) is taken so that the energy density at the center of the fireball at zero impact parameter is  $107 \text{ GeV}/\text{fm}^3$  at  $\tau_0 = 0.25 \text{ fm}/c$ . It corresponds to a temperature of  $510 \text{ MeV}$ , well above the critical temperature. The initial distributions for other impact parameters are obtained from geometrical scaling (2.8) only, with a contribution of binary collisions  $\alpha = 0.145$  [54]. This provides a satisfactory description of charged particle multiplicities for centralities 0–40%.

### III. EVOLUTION OF THE HOT MATTER

The numerical solution of Eqs. (2.6) is obtained as an evolution in proper time from initial densities (2.8). The total entropy ( $s$  is the entropy density)

$$S = \int \gamma \cosh(Y - \eta) s dx dx d\eta \quad (3.1)$$

is conserved to the accuracy of less than 0.5%. At the very beginning of the evolution a very rapid longitudinal expansion occurs (Fig. 2). The matter at the edges of the plateau of the energy density distribution is subject to longitudinal acceleration and eventually the distribution becomes approximately a Gaussian, that grows wider in time. The longitudinal acceleration is known to depend on the equation of state [55] and on possible viscosity effects [56]. For the perfect fluid and a hard equation of state the longitudinal expansion and acceleration is significant [55]. An effect not taken into account in the present calculation, that could modify the longitudinal acceleration at large rapidities, is the increase of the baryon chemical potential [50,51] resulting in a change of the equation of state.

For comparison we calculate a hydrodynamic evolution of the system assuming a 2 + 1D boost invariant expansion, with the energy density profile in the transverse plane given by Eq. (2.8), but without  $\eta$  dependence. The temperature at the center of the fireball ( $T = 485 \text{ MeV}$  for  $b = 0$ ) that reproduces the observed spectra is slightly lower than in the 3 + 1D case. This is the effect of the additional cooling in the non-boost invariant geometry due to the longitudinal acceleration. In 3 + 1D the longitudinal fluid rapidity is larger than in the Bjorken scaling solution (Fig. 3). At the center of the fireball the temperature drops down following the Bjorken formula  $T \propto \tau^{-c_s^2}$  (Fig. 4) up to  $\tau = 2\text{--}3 \text{ fm}/c$ . Later cooling from the transverse expansion and in the case of 3 + 1D additional longitudinal cooling set in. As a result the life-time of the 2 + 1D and 3 + 1D systems is very similar, in spite of the fact that in the later case the initial energy density is a factor 1.25 higher.

The hydrodynamic evolution is followed until freeze-out, that is assumed to happen at fixed temperature, with particles emitted from the freeze-out hypersurface without further rescattering. In the following, we present results for two

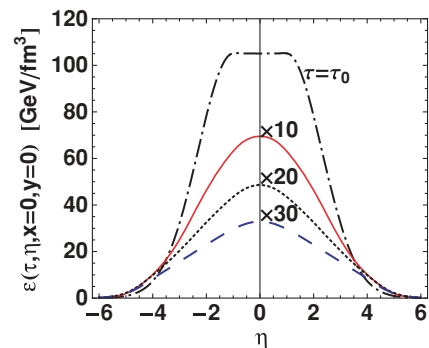


FIG. 2. (Color online) Energy density as function of space-time rapidity for different proper times  $\tau = 0.25, 2, 4, 6 \text{ fm}/c$  (dashed-dotted, solid, dotted, and dashed lines, respectively).

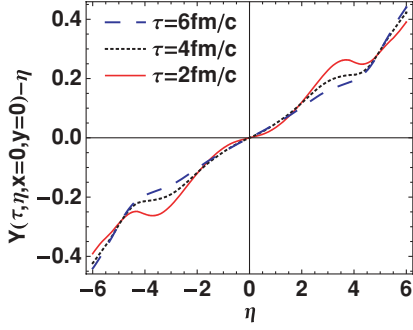


FIG. 3. (Color online) Deviation of the longitudinal fluid rapidity from the Bjorken flow  $Y(\tau, \eta, x, y) - \eta$  for different proper times  $\tau = 2, 4, 6$  fm/c (solid, dotted, and dashed lines, respectively).

different freeze-out temperatures  $T_f = 150$  and  $165$  MeV. The freeze-out hypersurface is a three-dimensional surface in  $\tau, \eta, x, y$  coordinates. Its shape can be deformed due to a strong collective flow and is deformed in the  $\eta - x$  direction due to the shift in the space-time rapidity in the initial conditions (2.13). In Figs. 5 and 6 is shown a cut ( $\tau - x$ ) through the freeze-out hypersurface at the freeze-out temperature  $T_f = 150$  MeV. At the central space-time rapidity  $\eta = 0$  the freeze-out hypersurfaces in the 3 + 1D and 2 + 1D calculations are very similar. For central collisions the dense system exists for 10 fm/c. This short life-time of the fireball results in values of extracted HBT radii compatible with the experiment. For large space-time rapidities the transverse size and the life-time of the fireball is smaller. The asymmetric shape of the freeze-out hypersurface for  $\eta \neq 0$  is the result of the tilt in the initial flow of the matter [Eq. (2.13)].

Most general freeze-out hypersurfaces realized in the hydrodynamic expansion can be parametrize using three angles:

$$\begin{aligned} \tau_{HS} &= d(\theta, \zeta, \phi) \sin \zeta \sin \theta + \tau_0, \\ \eta_{HS} &= \frac{d(\theta, \zeta, \phi)}{\Lambda} \cos \theta, \\ x_{HS} &= d(\theta, \zeta, \phi) \cos \zeta \sin \theta \cos \phi, \\ y_{HS} &= d(\theta, \zeta, \phi) \cos \zeta \sin \theta \sin \phi; \end{aligned}$$

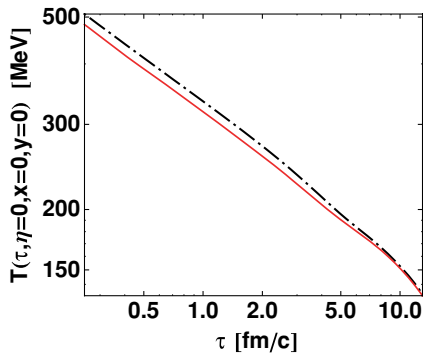


FIG. 4. (Color online) Temperature at the center of the fireball as function of the proper time from the 3 + 1D (dashed-dotted line) and from the 2 + 1D (solid line) evolutions ( $b = 2.1$  fm).

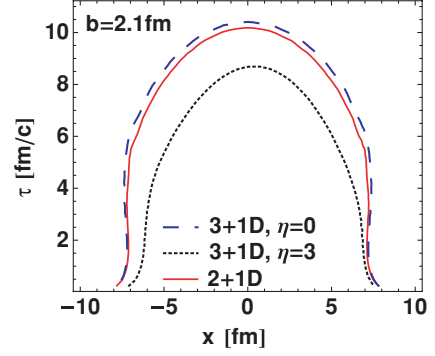


FIG. 5. (Color online) Freeze-out hypersurface  $T_f = 150$  MeV, for the impact parameter  $b = 2.1$  fm in the plane  $(t - x)$ ,  $y = 0$ , for  $\eta = 0$  (dashed line) and  $\eta = 3$  (dotted line). The solid line represents the freeze-out hypersurface for the 2 + 1D evolution.

$$\begin{aligned} 0 &\leq \theta \leq \pi, \\ 0 &\leq \zeta \leq \pi/2, \\ 0 &\leq \phi < 2\pi, \end{aligned} \quad (3.2)$$

$\Lambda$  is a constant length.

Following the Cooper-Frye prescription [57], particle spectra are given by

$$E \frac{d^3 N}{dp^3} = \int d\Sigma_\mu p^\mu f(p_\mu u^\mu). \quad (3.3)$$

$d\Sigma_\mu = \epsilon_{\mu\nu\alpha\beta} \partial_\theta x^\nu \partial_\zeta x^\alpha \partial_\phi x^\beta d\theta d\zeta d\phi$  is the integration element on the freeze-out hypersurface and  $f$  is the equilibrium Bose or Fermi momentum distribution. The four-momentum of the emitted particle is

$$p^\mu = (m_\perp y, p_\perp \cos \phi_p, p_\perp \sin \phi_p, m_\perp y), \quad (3.4)$$

and

$$p_\mu u^\mu = m_\perp \gamma \cosh(Y - y) - p_\perp (u_x \cos \phi_p + u_y \sin \phi_p), \quad (3.5)$$

$$\begin{aligned} d\Sigma_\mu p^\mu &= \frac{1}{\Lambda} d^2 \sin \theta (\cos \zeta d^2 \sin \zeta (p_\perp \cos \zeta \cos(\phi - \phi_p) \\ &+ m_\perp \cosh(y - \eta_{HS}) \sin \zeta) \sin^3 \theta \\ &- \cos \zeta \sin \theta (p_\perp \tau_0 \cos \zeta \cos \theta \cos(\phi - \phi_p)) \end{aligned}$$

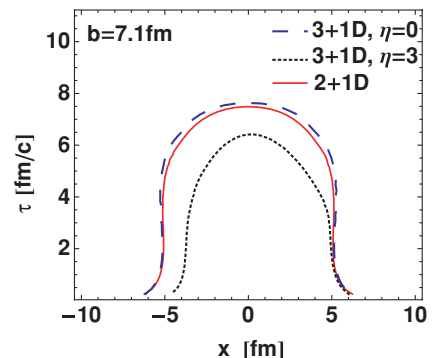


FIG. 6. (Color online) Same as Fig. 5 but for  $b = 7.1$  fm.

$$\begin{aligned}
 & + m_{\perp}(\tau_0 \cos \theta \cosh(y - \eta_{HS}) \sin \zeta \\
 & - \Lambda \sin \theta \sinh(y - \eta_{HS})) \partial_{\theta} d \\
 & + \tau_0(\cos \zeta(-m_{\perp} \cos \zeta \cosh(y - \eta_{HS}) \\
 & + p_{\perp} \cos(\phi - \phi_p) \sin \zeta) \partial_{\zeta} d + p_{\perp} \sin(\phi - \phi_p) \partial_{\phi} d) \\
 & + d \sin \theta(\cos \zeta(p_{\perp} \tau_0 \cos \zeta \cos(\phi - \phi_p) \sin \theta \\
 & + m_{\perp}(\tau_0 \cosh(y - \eta_{HS}) \sin \zeta \sin \theta \\
 & + \Lambda \cos \theta \sinh(y - \eta_{HS})) \\
 & + \sin \zeta(-\cos \zeta \cos \theta(p_{\perp} \cos \zeta \cos(\phi - \phi_p) \\
 & + m_{\perp} \cosh(y - \eta_{HS}) \sin \zeta) \sin \theta \partial_{\theta} d \\
 & + \cos \zeta(-m_{\perp} \cos \zeta \cosh(y - \eta_{HS}) \\
 & + p_{\perp} \cos(\phi - \phi_p) \sin \zeta) \partial_{\zeta} d \\
 & + p_{\perp} \sin(\phi - \phi_p) \partial_{\phi} d)) d \theta d \zeta d \phi. \quad (3.6)
 \end{aligned}$$

After the hydrodynamic evolution, the three-dimensional hypersurface parametrized by the variables  $\theta, \zeta, \phi$  is exported to the statistical emission and resonance decay code THERMINATOR [58]. The density (3.3) [with Eqs. (3.5) and (3.6)] is implemented in the code. THERMINATOR generates events in two steps. First 380 different kind of particles and resonances emitted from the hypersurface are generated according to the density (3.3), then resonances are allowed to decay.

#### IV. PARTICLE SPECTRA, FLOW, CORRELATION RADII

Charged particle distributions in pseudorapidity  $\eta_{PS} = \frac{1}{2} \log\left(\frac{p^+ p_z}{p^- p_z}\right)$  have been measured for different centralities. The 3+1D hydrodynamic model can reproduce the data for centralities 0–40% (Fig. 7). We show results for two freeze-out temperatures  $T_f = 165$  and 150 MeV. The first one is close to the estimate of the chemical freeze-out temperature in Au-Au collisions [5,7,8]. When decreasing the freeze-out temperature particle multiplicity goes down, but the effect

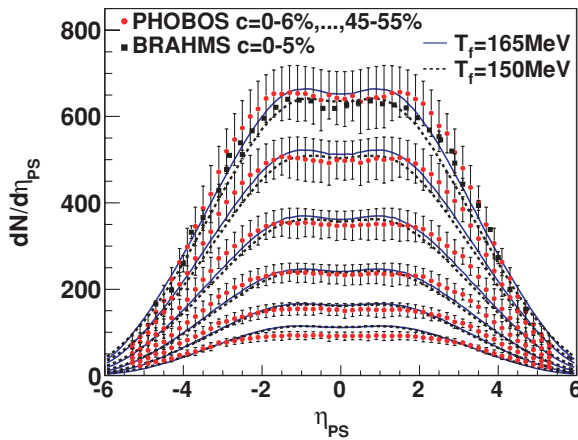


FIG. 7. (Color online) Pseudorapidity distribution of charged particles for centrality classes 0–6%, 6–15%, 15–25%, 25–35%, 35–45%, and 45–55% calculated for the freeze-out temperatures  $T_f = 165$  and 150 MeV (solid and dashed lines, respectively) compared to PHOBOS Collaboration data (dots) [59]. The squares represent the BRAHMS Collaboration data for centrality 0–5% [60].

is small. It gives confidence to our model, that assumes a chemically equilibrated fluid down to  $T_f = 150$  MeV. For lower freeze-out temperatures the difference between a chemically equilibrated and a partially equilibrated fluid becomes significant [27]. The centrality dependence that we predict comes solely from the geometrical scaling of the fireball density according to Eq. (2.8), other parameters (in particular the freeze-out temperature) remain unchanged. On general grounds, one expects the hydrodynamic model to break down for very peripheral collisions. The interaction region in peripheral collisions is not dense enough to equilibrate completely. Experimental data on the centrality dependence of strangeness production and of particle spectra suggest that at impact parameters  $b > 9$  fm [61–63] less than 70% of the interaction region can be treated as a thermally equilibrated fireball.

For central collisions  $c = 0$ –5% we calculate the transverse momentum spectra of pions and kaons at different rapidities. In the whole rapidity range where identified particle spectra are available [53], we find an excellent agreement between the results of the hydrodynamic evolution coupled with statistical emission and the BRAHMS Collaboration data (Figs. 8 and 9). The best agreement is achieved for a freeze-out temperature of 150 MeV. This very good agreement between the data and the hydrodynamic model indicates that the matter created in central collisions behaves as a thermally equilibrated (in the rapidity range  $-3.5 < y < 3.5$ ) although not boost-invariant fireball.

A different way of testing thermalization in Au-Au collisions is to compare predictions and experimental data for transverse momentum spectra at different centralities. In Fig. 10 are shown  $\pi^+$  spectra for  $p_{\perp}$  up to 3 GeV/c and centralities in the range 0–50%. We find that hydrodynamic calculations

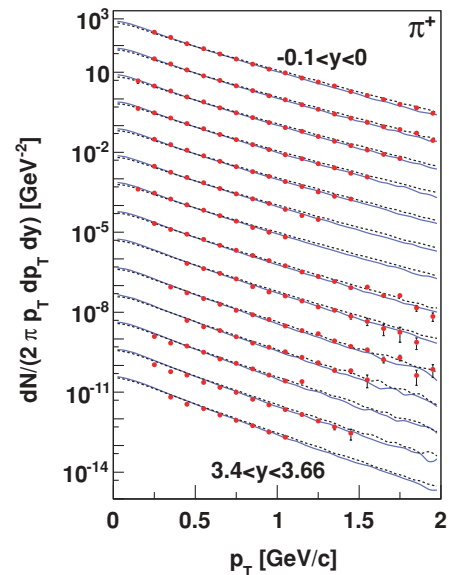


FIG. 8. (Color online) Transverse momentum spectra of  $\pi^+$  for different rapidity windows ranging from  $-0.1 < y < 0$  to  $3.4 < y < 3.66$  for centrality 0–5% (results for different rapidity bins are scaled down by powers of 1/10). The dots represent the data of the BRAHMS Collaboration [53].

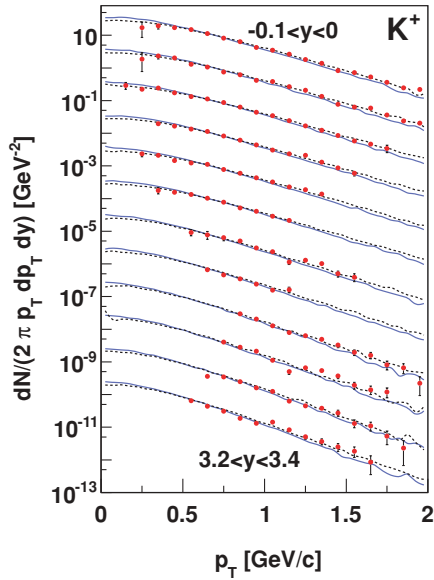


FIG. 9. (Color online) Transverse momentum spectra of  $K^+$  for different rapidity windows ranging from  $-0.1 < y < 0$  to  $3.2 < y < 3.4$  for centrality 0–5% (results for different rapidity bins are scaled down by powers of  $1/10$ ). The dots represent the data of the BRAHMS Collaboration [53].

with  $T_f = 150$  MeV are in very good agreement with the experiment for all centralities and transverse momenta  $p_\perp < 2$  GeV/c. Pions with higher transverse momenta originate mostly from hard processes and cannot be described as emitted thermally from a collectively expanding fluid. The agreement between the experimental spectra and the results of the calculation for  $K^+$  (Fig. 11) is limited to centralities 0–30%. For centrality bins 30–40% and 40–50% the calculation

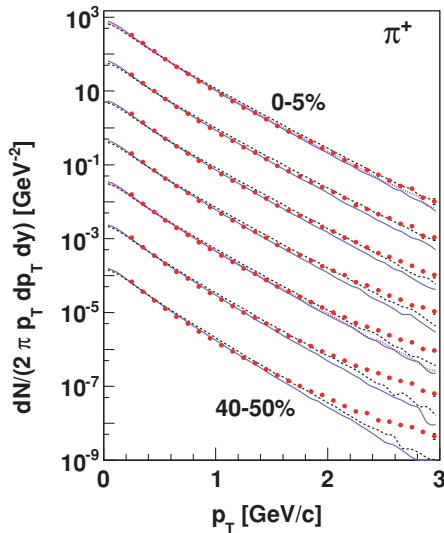


FIG. 10. (Color online) Transverse momentum spectra of  $\pi^+$  for different centrality classes 0–5%, 5–10%, 10–15%, 15–20%, 20–30%, 30–40%, and 40–50% (results for different centralities are scaled down by powers of  $1/10$ ) calculated for the freeze-out temperatures  $T_f = 165$  and  $150$  MeV (solid and dashed lines, respectively) compared to PHENIX Collaboration data (dots) [64].

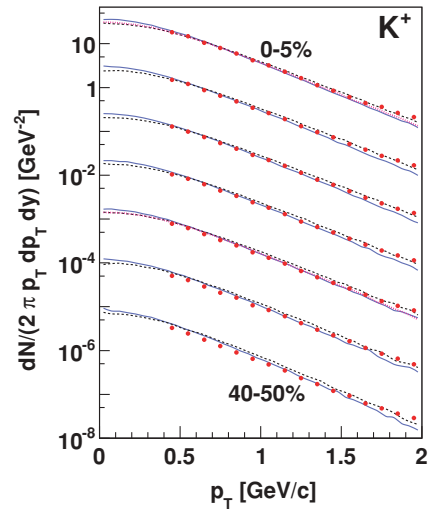


FIG. 11. (Color online) Same as Fig. 10 but for  $K^+$ .

overpredicts the kaon multiplicity, even though the slope of the spectra is similar in the model and in the data. The reduced strangeness production in peripheral collisions can be an effect of energy and momentum conservation [65], canonical suppression [66], or reduced size of the thermally equilibrated fireball [61,63]. In Figs. 10 and 11 are also shown the results of a  $2 + 1D$  hydrodynamic calculation for two centralities 0–5% and 20–30% (dotted lines, indistinguishable from the  $3 + 1D$  results). The resulting spectra for central rapidities are very similar to the ones from the  $3 + 1D$  calculations, but are obtained after the expansion of the matter with smaller initial energy density.

The elliptic flow represents a very sensitive probe of the collective behavior of the dense matter [18]. The azimuthal asymmetry with respect to the reaction plane is described by the elliptic flow coefficient  $v_2$

$$\frac{dN}{p_\perp dp_\perp d\phi_p} = \frac{dN}{p_\perp dp_\perp} (1 + 2v_2(p_\perp) \cos(2\phi_p) + \dots). \quad (4.1)$$

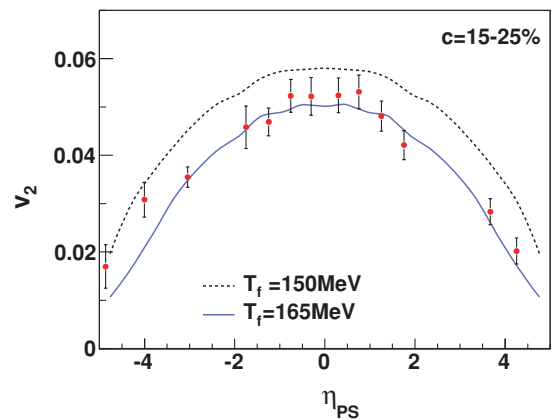


FIG. 12. (Color online) Pseudorapidity dependence of the elliptic flow coefficient for charged particles for centralities 15–25% for freeze-out temperatures  $T_f = 150$  and  $165$  MeV (dashed and solid lines, respectively), data for the PHOBOS Collaboration are denoted by dots [52].

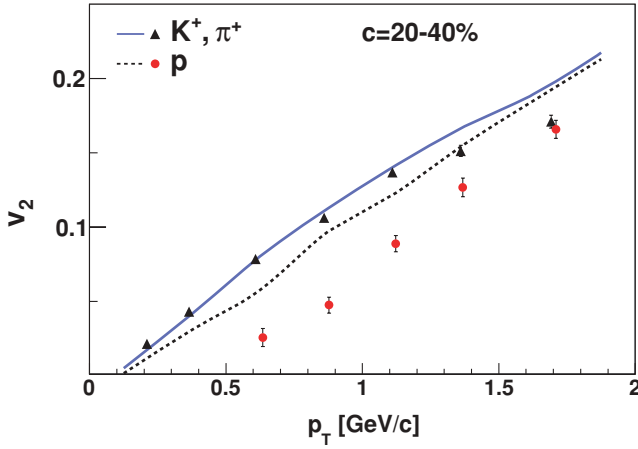


FIG. 13. (Color online) Transverse momentum dependence of the elliptic flow coefficient for protons (dotted line and dots) and for  $\pi^+$  and  $K^+$  (solid line and triangles). Calculations are performed for  $T_f = 150$  MeV, data are from the PHENIX Collaboration [67].

The elliptic flow coefficient for charged particles has been measured for a broad range of pseudorapidities [52], showing a strong pseudorapidity dependence. There is no sign of a Bjorken plateau for central rapidities. To reproduce the shape of the  $v_2$  pseudorapidity dependence, initial conditions in energy density with a relatively narrow plateau in space-time rapidity must be chosen [Eq. (2.12)] [14,33]. Such initial conditions, combined with a hard equation of state and an early initial time of the evolution result in a complete disappearance of the Bjorken plateau in the final hadron distributions. It must be stressed however, that it does not mean that for noncentral rapidities the evolution is not described by hydrodynamics and statistical emission. The model works very well and describes the observed spectra for  $-3.5 < y < 3.5$  (Figs. 8 and 9). The longitudinal expansion and the smaller size of the system at non-zero space-time rapidities reduce the final elliptic flow. The elliptic flow as function of  $p_\perp$  for identified particles is shown in Fig. 13. Hydrodynamic calculations describe the elliptic flow for mesons with  $p_\perp < 1.5$  GeV/c, but to reproduce the saturation of  $v_2$  for large  $p_\perp$  dissipative or viscosity effects must be invoked. The elliptic flow for baryons is overpredicted for the freeze-out temperatures chosen.

Pairs of identical particles emitted from the thermal source can be used to extract the size of the fireball from the interferometry measurement [69–72]. The statistical emission code THERMINATOR [58] provides the space-time points of particle creation. For a set of generated events the correlation function is constructed from same-event and mixed-event pairs [73]. Such a general procedure allows for an easy implementation of experimental cuts, final interaction or Coulomb corrections [74,75] and can be also applied to non-identical particle correlations [76]. The extracted multidimensional correlation functions are parametrized by the Bertsch-Pratt formula [77,78]

$$C(k_\perp, q_{\text{out}}, q_{\text{side}}, q_{\text{long}}) = 1 + \lambda \exp(-R_{\text{side}}^2 q_{\text{side}}^2 - R_{\text{out}}^2 q_{\text{out}}^2 - R_{\text{long}}^2 q_{\text{long}}^2). \quad (4.2)$$

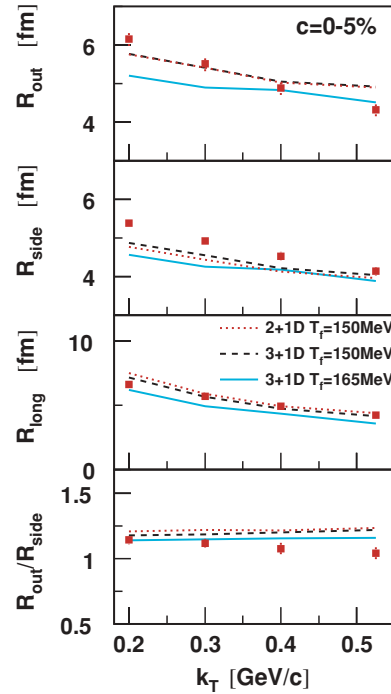


FIG. 14. (Color online) HBT radii for Au-Au collisions at centrality 0–5%. 3 + 1D calculations with  $T_f = 165$  MeV (solid line) and  $T_f = 150$  MeV (dashed line), 2 + 1D calculation with  $T_f = 150$  MeV (dotted line) and STAR Collaboration data [68] (squares) are shown.

The fit parameters  $R$  (HBT radii) are extracted for fixed bins of pair total transverse momenta  $k_\perp$ . The experimental radii  $R_{\text{out}}$ ,  $R_{\text{side}}$ , and  $R_{\text{long}}$  are well described by the hydrodynamic calculations with  $T_f = 150$  MeV (Fig. 14). We notice that the 3 + 1D and 2 + 1D calculations that both describe the transverse momentum spectra, give also very similar HBT radii. Similarity in the spectra means that the transverse collective flow is the same; together with the similarity in the freeze-out hypersurfaces (Fig. 5) it explains why the HBT radii from the 3 + 1D and 2 + 1D evolutions come out so close. The discrepancies between the calculations and the data are smaller than 10%. The ratio  $R_{\text{out}}/R_{\text{side}}$  from the model comes out close to the data as well. This remarkable property of modern hydrodynamic calculations, which solves the so-called RHIC HBT puzzle, has been noticed in Ref. [26] based on 2 + 1D simulations. The present study is the first 3 + 1D calculation using the same equation of state and an early initial time.

## V. CONCLUSIONS

We present an extensive study of the 3 + 1D hydrodynamic model of the evolution of the fireball. Compared to other similar calculations we use a different equation of state [48] and an early initial time to start up the expansion. As a result we find a very good agreement between the calculated transverse momentum spectra for pions and kaons for different centralities and a broad range of rapidities. The fireball formed in Au-Au collisions at  $\sqrt{s} = 200$  GeV is thermalized for centralities 0–40%. The result is remarkable, since we use

an energy density profile for different impact parameters predicted from the Glauber model geometrical scaling, with an overall normalization fixed for most central collisions. It is not surprising that for peripheral collisions this scaling breaks down [62], and we overpredict the size of the thermalized fireball. The thermal description of the production of strange particles is subject to even more restrictions. As a result the spectra of kaons are well reproduced for centralities 0–30%. For more peripheral collisions the number of observed kaons is smaller than predicted in the model, signaling an incomplete chemical equilibration of the interaction region.

The calculation reproduces the observed spectra up to transverse momenta of 2 GeV/c, in a wider range than most of the previous calculations. This indicates that a long hydrodynamical evolution generates the correct amount of collective flow. For central collisions we obtain an excellent description of pion and kaon spectra for noncentral rapidities. This demonstrates that the fireball is thermalized and that particle production is statistical for all rapidities in the range  $\pm 3.5$  units. This confirms in a dynamical calculation the applicability of the thermal fits from Refs. [50,51]. However, the rapidity dependence of the baryon chemical potential found in these fits cannot be described in our hydrodynamic model without explicit baryon current. The elliptic flow shows a strong pseudorapidity dependence, that can be reproduced assuming a collective thermal evolution but with reduced initial energy density at nonzero space-time rapidities.

Another important result is the satisfactory description of pion interferometry radii. Assuming a rapid expansion of the system, the right amount of transverse flow and a reasonable life-time of the fireball are obtained. This gives HBT radii  $R_{out}$ ,  $R_{side}$ , and  $R_{long}$  similar as in the experiment. The ratios  $R_{out}/R_{side}$  come out to within less than 10% of the measured values. We also show that very similar HBT radii can be obtained from a 2 + 1D hydrodynamic calculation with correctly chosen initial conditions. It must be stressed however, that the initial energy density that reproduces the experimental spectra and HBT radii is 86 GeV/fm<sup>3</sup> at the maximum in 2 + 1D, whereas it is 107 GeV/fm<sup>3</sup> in 3 + 1D. As mentioned, our 3 + 1D calculation describes particle emission at nonzero rapidities as well.

### ACKNOWLEDGMENTS

Discussions with Mikołaj Chojnacki, Wojtek Florkowski, and Tetsufumi Hirano are gratefully acknowledged. The authors thank Adam Kisiel for providing the pair correlations analysis code. This work was supported by Polish Ministry of Science and Higher Education under Grant No. N202 034 32/0918.

### APPENDIX: DEPENDENCE ON THE INITIAL TIME AND THE EQUATION OF STATE

In this section results obtained by modifying the parameters of the initial state in the hydrodynamic evolution are presented. The quality of our description of the experimental data relies on the chosen early initial time of the evolution  $\tau_0 = 0.25$  fm/c

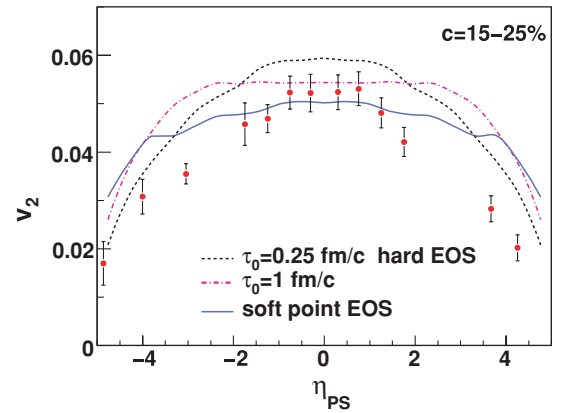


FIG. 15. (Color online) Pseudorapidity dependence of the elliptic flow coefficient for charged particles for centralities 15–25% for  $\tau_0 = 0.25$  fm/c and a soft equation of state (solid line), for  $\tau_0 = 1$  fm/c and the default equation of state (dashed-dotted line) compared to the default choice of parameters (dashed line), data for the PHOBOS Collaboration are denoted by dots [52].

and the relatively hard equation of state. To check the dependence of the results on these choices we perform two additional calculations: the first one with a larger initial time  $\tau_0 = 1$  fm/c and the same velocity of sound and a second one with  $\tau_0 = 0.25$  fm/c but with a velocity of sound corresponding to a softening of the equation of state at the critical temperature (dashed line in Fig. 1). First the initial densities for the hydrodynamic evolution are adjusted to

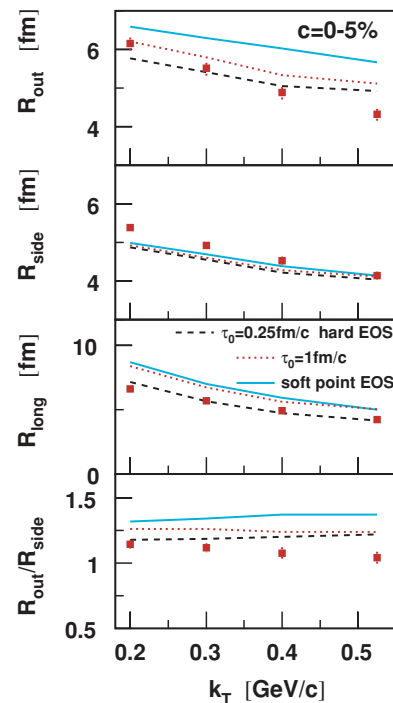


FIG. 16. (Color online) HBT radii for Au-Au collisions at centrality 0–5%. 3 + 1D calculations with  $\tau_0 = 0.25$  fm/c and a soft equation of state (solid line), for  $\tau_0 = 1$  fm/c and the default equation of state (dotted line) compared to the default choice of parameters (dashed line), STAR Collaboration data [68] are shown by squares.

reproduce the final spectra and charged particle multiplicities. The energy density profile is taken of the same form as in the default calculation [Eq. (2.8)], but with modified parameters. When the starting time is increased to 1 fm/c the initial temperature must be reduced, the parameter  $\epsilon_0$  corresponds in this case to a temperature of 330 MeV, also the longitudinal profile should have a broader plateau with  $\eta_0 = 1.4$ , the freeze-out temperature is  $T_f = 140$  MeV. Following the same methodology, in the evolution using the equation of state with a softening around  $T_c$  we find the maximal temperature 425 MeV, the plateau half-width  $\eta_0 = 1.2$  and the freeze-out temperature 140 MeV. With these choices the distribution  $dN/d\eta$  of charged particles and the transverse momentum spectra of pions and kaons are reproduced.

With the initial conditions fixed by the multiplicity and transverse momentum spectra, predictions of the hydrodynamic model for the elliptic flow and the HBT radii can be made. In Fig. 15 are shown the results for the pseudorapidity dependence of the elliptic flow coefficient for charged particles. The reduced evolution time for the case with  $\tau_0 = 1$  fm/c

and the reduced longitudinal acceleration for the case of the soft point equation of state require the use of a broader initial distribution of matter in the space-time rapidity. This leads to a reduced dependence of  $v_2$  on pseudorapidity, with a noticeable flattening in the central region (solid and dashed-dotted lines in Fig. 15). The form of the pseudorapidity dependence obtained with the default, hard equation of state and early start up time follows closer the experimental data (Fig. 12).

The interferometry radii are sensitive to the size, flow and life-time of the emitting source. It has been advocated that a change in the evolution due to a first order phase transition would lead a strong increase of the ratio  $R_{\text{out}}/R_{\text{side}}$  [79]. The moderate softening of the equation of state considered in this section is not a first order phase transition, but still it leads an increase of the above mentioned ratio (solid line in Fig. 16). Also a latter start up time of the evolution means that the fireball has to live longer to accumulate the right amount of collective flow and the agreement with the HBT data worsens. Both modification of the initial conditions discussed in this section lead an overshooting of the measured  $R_{\text{long}}$  radii.

- 
- [1] I. Arsene *et al.* (BRAHMS Collaboration), Nucl. Phys. **A757**, 1 (2005).
- [2] B. B. Back *et al.* (PHOBOS Collaboration), Nucl. Phys. **A757**, 28 (2005).
- [3] J. Adams *et al.* (STAR Collaboration), Nucl. Phys. **A757**, 102 (2005).
- [4] K. Adcox *et al.* (PHENIX Collaboration), Nucl. Phys. **A757**, 184 (2005).
- [5] P. Braun-Munzinger, D. Magestro, K. Redlich, and J. Stachel, Phys. Lett. **B518**, 41 (2001).
- [6] A. Andronic, P. Braun-Munzinger, and J. Stachel, Nucl. Phys. **A772**, 167 (2006).
- [7] J. Cleymans, B. Kampfer, M. Kaneta, S. Wheaton, and N. Xu, Phys. Rev. C **71**, 054901 (2005).
- [8] W. Florkowski, W. Broniowski, and M. Michalec, Acta Phys. Pol. B **33**, 761 (2002).
- [9] J. Rafelski, J. Letessier, and G. Torrieri, Phys. Rev. C **72**, 024905 (2005).
- [10] F. Becattini, J. Manninen, and M. Gazdzicki, Phys. Rev. C **73**, 044905 (2006).
- [11] E. Schnedermann, J. Sollfrank, and U. W. Heinz, Phys. Rev. C **48**, 2462 (1993).
- [12] P. F. Kolb, J. Sollfrank, and U. W. Heinz, Phys. Rev. C **62**, 054909 (2000).
- [13] S. A. Bass and A. Dumitru, Phys. Rev. C **61**, 064909 (2000).
- [14] C. Nonaka and S. A. Bass, Phys. Rev. C **75**, 014902 (2007).
- [15] J.-Y. Ollitrault, Phys. Rev. D **46**, 229 (1992).
- [16] D. Teaney, J. Lauret, and E. V. Shuryak, Phys. Rev. Lett. **86**, 4783 (2001).
- [17] P. Huovinen, P. F. Kolb, U. W. Heinz, P. V. Ruuskanen, and S. A. Voloshin, Phys. Lett. **B503**, 58 (2001).
- [18] S. A. Voloshin, A. M. Poskanzer, and R. Snellings (2008) arXiv:0809.2949.
- [19] B. B. Back *et al.* (PHOBOS Collaboration), Phys. Rev. Lett. **91**, 072302 (2003).
- [20] S. S. Adler *et al.* (PHENIX Collaboration), Phys. Rev. Lett. **91**, 072303 (2003).
- [21] J. Adams *et al.* (STAR Collaboration), Phys. Rev. Lett. **91**, 072304 (2003).
- [22] I. Arsene *et al.* (BRAHMS Collaboration), Phys. Rev. Lett. **91**, 072305 (2003).
- [23] M. Gyulassy and M. Plumer, Phys. Lett. **B243**, 432 (1990).
- [24] R. Baier, D. Schiff, and B. G. Zakharov, Annu. Rev. Nucl. Part. Sci. **50**, 37 (2000).
- [25] C. Nonaka, J. Phys. G **34**, S313 (2007).
- [26] W. Broniowski, M. Chojnacki, W. Florkowski, and A. Kisiel, Phys. Rev. Lett. **101**, 022301 (2008).
- [27] T. Hirano and K. Tsuda, Phys. Rev. C **66**, 054905 (2002).
- [28] T. Hirano, K. Morita, S. Muroya, and C. Nonaka, Phys. Rev. C **65**, 061902(R) (2002).
- [29] P. F. Kolb and U. W. Heinz, in *Quark Gluon Plasma 3*, edited by R. Hwa and X. N. Wang (World Scientific, Singapore, 2004), nucl-th/0305084.
- [30] P. Huovinen, in *Quark Gluon Plasma 3*, edited by R. Hwa and X. N. Wang (World Scientific, Singapore, 2004), nucl-th/0305064.
- [31] Y. Hama *et al.*, Nucl. Phys. **A774**, 169 (2006).
- [32] P. Huovinen and P. V. Ruuskanen, Annu. Rev. Nucl. Part. Sci. **56**, 163 (2006).
- [33] T. Hirano, U. W. Heinz, D. Kharzeev, R. Lacey, and Y. Nara, Phys. Lett. **B636**, 299 (2006).
- [34] T. Hirano, U. W. Heinz, D. Kharzeev, R. Lacey, and Y. Nara, J. Phys. G **34**, S879 (2007).
- [35] T. Hirano, N. van der Kolk, and A. Bilandzic (2008), arXiv:0808.2684.
- [36] R. P. G. Andrade, F. Grassi, Y. Hama, T. Kodama, and W. L. Qian, Phys. Rev. Lett. **101**, 112301 (2008).
- [37] S. V. Akkelin, Y. Hama, I. A. Karpenko, and Y. M. Sinyukov, Phys. Rev. C **78**, 034906 (2008).
- [38] J. D. Bjorken, Phys. Rev. D **27**, 140 (1983).
- [39] C. E. Aguiar, Y. Hama, T. Kodama, and T. Osada, Nucl. Phys. **A698**, 639 (2002).
- [40] K. Morita and S. Muroya, Prog. Theor. Phys. **111**, 93 (2004).
- [41] K. Morita, Braz. J. Phys. **37**, 1039 (2007).
- [42] A. Muronga, Phys. Rev. Lett. **88**, 062302 (2002).

- [43] H. Song and U. W. Heinz, Phys. Lett. **B658**, 279 (2008).  
[44] A. Muronga, Phys. Rev. C **76**, 014909 (2007).  
[45] R. Baier and P. Romatschke, Eur. Phys. J. C **51**, 677 (2007).  
[46] P. Romatschke and U. Romatschke, Phys. Rev. Lett. **99**, 172301 (2007).  
[47] A. K. Chaudhuri, Phys. Rev. C **74**, 044904 (2006).  
[48] M. Chojnacki and W. Florkowski, Acta Phys. Pol. B **38**, 3249 (2007).  
[49] M. Chojnacki, W. Florkowski, W. Broniowski, and A. Kisiel, Phys. Rev. C **78**, 014905 (2008).  
[50] B. Biedron and W. Broniowski, Phys. Rev. C **75**, 054905 (2007).  
[51] F. Becattini, J. Cleymans, and J. Strumpfer, PoS **CPOD07**, 012 (2007).  
[52] B. B. Back *et al.* (PHOBOS Collaboration), Phys. Rev. C **72**, 051901(R) (2005).  
[53] I. G. Bearden *et al.* (BRAHMS Collaboration), Phys. Rev. Lett. **94**, 162301 (2005).  
[54] B. B. Back *et al.* (PHOBOS Collaboration), Phys. Rev. C **70**, 021902(R) (2004).  
[55] L. M. Satarov, I. N. Mishustin, A. V. Merdeev, and H. Stöcker, Phys. Rev. C **75**, 024903 (2007).  
[56] P. Bozek, Phys. Rev. C **77**, 034911 (2008).  
[57] F. Cooper and G. Frye, Phys. Rev. D **10**, 186 (1974).  
[58] A. Kisiel, T. Taluc, W. Broniowski, and W. Florkowski, Comput. Phys. Commun. **174**, 669 (2006).  
[59] B. B. Back *et al.*, Phys. Rev. Lett. **91**, 052303 (2003).  
[60] I. G. Bearden *et al.* (BRAHMS Collaboration), Phys. Rev. Lett. **88**, 202301 (2002).  
[61] P. Bozek, Acta Phys. Pol. B **36**, 3071 (2005).  
[62] P. Bozek (2008), arXiv:0811.1918.  
[63] F. Becattini and J. Manninen, Phys. Lett. **B673**, 19 (2009).  
[64] S. S. Adler *et al.* (PHENIX Collaboration), Phys. Rev. C **69**, 034909 (2004).  
[65] Z. Chajecki and M. Lisa, Phys. Rev. C **79**, 034908 (2009).  
[66] S. Hamieh, K. Redlich, and A. Tounsi, Phys. Lett. **B486**, 61 (2000).  
[67] S. S. Adler *et al.* (PHENIX Collaboration), Phys. Rev. Lett. **91**, 182301 (2003).  
[68] J. Adams *et al.* (STAR Collaboration), Phys. Rev. C **71**, 044906 (2005).  
[69] U. W. Heinz and B. V. Jacak, Annu. Rev. Nucl. Part. Sci. **49**, 529 (1999).  
[70] U. A. Wiedemann and U. W. Heinz, Phys. Rep. **319**, 145 (1999).  
[71] R. M. Weiner, Phys. Rep. **327**, 249 (2000).  
[72] M. A. Lisa, S. Pratt, R. Soltz, and U. Wiedemann, Annu. Rev. Nucl. Part. Sci. **55**, 357 (2005).  
[73] A. Kisiel, W. Florkowski, W. Broniowski, and J. Pluta, Phys. Rev. C **73**, 064902 (2006).  
[74] M. G. Bowler, Phys. Lett. **B270**, 69 (1991).  
[75] Y. Sinyukov, R. Lednicky, S. V. Akkelin, J. Pluta, and B. Erasmus, Phys. Lett. **B432**, 248 (1998).  
[76] A. Kisiel, Braz. J. Phys. **37**, 917 (2007).  
[77] S. Pratt, Phys. Rev. D **33**, 1314 (1986).  
[78] G. Bertsch, M. Gong, and M. Tohyama, Phys. Rev. C **37**, 1896 (1988).  
[79] D. H. Rischke and M. Gyulassy, Nucl. Phys. **A608**, 479 (1996).